Supported Binary Oxide Catalysts Containing CuO Coupled with Ga_2O_3 and SnO_2

S. Bennici,[†] A. Auroux,[§] C. Guimon,[#] and A. Gervasini*[,†,‡]

Dipartimento di Chimica Fisica ed Elettrochimica, Università degli Studi di Milano, Centro di Eccellenza CIMAINA, via C. Golgi n. 19, 20133 Milano, Italy, Institut de Recherches sur la Catalyse, CNRS, 2 av. A. Einstein, 69626 Villeurbanne Cedex, France, and UMR (CNRS) 5624, Université de Pau et des Pays de l'Adour, 2 av. du Président Angot, 64053 Pau Cedex 9, France

Received February 1, 2006. Revised Manuscript Received May 9, 2006

Two series of binary oxide catalysts (CuGa/SA and CuSn/SA) containing CuO coupled with Ga_2O_3 or SnO_2 were prepared by dispersing the metal phases onto a high surface area acidic silica−alumina (SA) support by an adsorption method. Similar total amounts of metals (about 1.6 $atom_{Met}\cdot nm^{-2}$) were deposited onto the support, in different proportions, to obtain samples with weight percent of copper varying from 3.3 to 6.5% The SA support was first covered by the copper precursor, $Cu(C_2H_3O_2)_2$, and then gallium ($Ga(NO_3)_3\cdot H_2O$) or tin ($SnCl_4\cdot 5H_2O$) precursors were deposited on the dried Cu-containing sample. The calcined materials were characterized by surface techniques (N_2 adsorption and XPS), to detect the surface morphology and chemical state of metal species, and by FT-IR and adsorption calorimetry after CO adsorption. Nanosized metal phases were observed in every case. Besides Cu(II), the surfaces contained Cu(I) as well as Cu(δ^+) ions (with $1 < \delta < 2$) stabilized by the interaction with the acid centers of the support. Gallium oxide preferentially covered the copper oxide phase, while tin dioxide mainly deposited on the bare surface of the support. The reducibility properties of the different supported metal oxides were investigated by TPR from both the qualitative and quantitative points of view. The catalytic performances of the simple and binary surfaces were comparatively studied in different reactions (decomposition and reduction of N_2O and NO, and CH_4 combustion) considered as test reactions to investigate the reducing or oxidizing properties of the materials. The observed differences in catalytic activity among the catalysts are discussed in relation with the surface composition and properties.

1. Introduction

The past decades have seen a great deal of effort in optimizing the preparation of amorphous catalysts containing copper oxide because of their promising applications to many reactions in environmental (NO_x reduction by hydrocarbon agents,[1−9] N_2O decomposition and reduction,[10,11] and CO oxidation[12−14]), primary (methanol synthesis,[15,16] oxidation,[17,18] steam-reforming,[18−20] alcohol dehydrogenation,[21,22] ketone hydrogenation,[23] and water−gas shift reaction[24,25]), and secondary (oxidative reactions of organics[26] and ester hydrogenolysis) chemistry. Because of the recognized benefits of nanosized copper oxide aggregates for improving the activity and especially the selectivity of some reactions, various methodologies of preparation of catalytic systems containing copper oxide in nanosized dimensions have been

* Corresponding author. E-mail: antonella.gervasini@unimi.it.
[†] Dipartimento di Chimica Fisica ed Elettrochimica, Università di Milano.
[‡] Centro di Eccellenza CIMAINA, Milano.
[§] Institut de Recherches sur la Catalyse, CNRS.
[#] UMR 5624, Université de Pau et des Pays de l'Adour.

(1) Chen, L.; Horiuchi, T.; Osaki, T.; Mori, T. *Appl. Catal., B* **1999**, *23*, 259−269.
(2) Bennici, S.; Carniti, P.; Gervasini, A. *Catal. Lett*. **2004**, *98*, 187−194.
(3) Bennici, S.; Gervasini, S.; Ravasio, N.; Zaccheria, F. *J. Phys. Chem. B* **2003**, *107*, 5168−5176.
(4) Morales, J.; Caballero, A.; Holgado, J. P.; Espinos, J. P.; Gonzalez-Elipe, A. R. *J. Phys. Chem. B* **2002**, *106*, 10185−10190.
(5) Gervasini, A.; Carniti, P. *Catal. Lett*. **2002**, *84*, 235−244.
(6) Carniti, P.; Gervasini, A.; Modica, V. H.; Ravasio, N. *Appl. Catal., B* **2000**, *28*, 175−185.
(7) Shibata, J.; Shimizu, K.; Satsuma, A.; Hattori, T. *Appl. Catal., B* **2002**, *37*, 197−204.
(8) Shimizu, K.; Maeshima, H.; Yoshida, H.; Satsuma, A.; Hattori, T. *Phys. Chem. Chem. Phys*. **2000**, *2*, 2435−2439.
(9) Pietrogiacomi, D.; Sannino, D.; Tuti, S.; Ciambelli, P.; Indovina, V.; Occhiuzzi, M.; Pepe, F. *Appl. Catal., B* **1999**, *21*, 141−150.
(10) Dandekar, A.; Vannice, M. A. *Appl. Catal., B* **1999**, *22*, 179−200.
(11) Bartley, G. J. J.; Burch, R.; Chappell, R. J. *Appl. Catal., A* **1988**, *43*, 91−104.
(12) Yu Yao, Y. F.; Kummer, J. T. *J. Catal*. **1977**, *46*, 388−401.
(13) Severino, F.; Brito, J.; Carías, O. *J. Catal*. **1986**, *102*, 172−179.
(14) Lopez Agudo, A.; Paacios, J. M.; Fierro, J. L. G.; Laine, J. Severino, F. *Appl. Catal*. **1992**, *91*, 43−55.
(15) Waugh, K. C. *Catal. Today* **1992**, *15*, 51−75.
(16) Gunter, M. M.; Ressler, T.; Bems, B.; Buscher, C.; Genger, T.; Hinrichsen, O.; Muhler, M.; Schlogl, R. *Catal. Lett.* **2001**, *71*, 37−44.
(17) Bluhm, H.; Havecker, M.; Knop-Gericke, A.; Kleimenov, E.; Schlogl, R.; Teschner, D.; Bukhtiyarov, V. I.; Ogletree, D. F.; Salmeron, M. *J. Phys. Chem. B* **2004**, *108*, 14340−14347.
(18) Agrell, J.; Birgersson, H.; Boutonnet, M.; Melian-Cabrera, I.; Navarro, R. M.; Fierro, J. L. G. *J. Catal*. **2003**, *219*, 389−403.
(19) Lindstrom, B.; Petterson, L. J.; Govind Menon, P. *Appl. Catal., A* **2002**, *234*, 111−125.
(20) Yao, C.-Z.; Wang, L.-C.; Liu, Y.-M.; Wu, G.-S.; Cao, Y.; Dai, W.-L.; He, H.-Y.; Fan, K.-N. *Appl. Catal., A* **2005**, *297*, 151−158.
(21) Guerreiro, E. D.; Gorriz, O. F.; Rivarola, J. B.; Arrua, L. A. *Appl. Catal., A* **1997**, *165*, 259−271.
(22) Tu, Y.-J.; Chen, Y.-W. *Ind. Eng. Chem. Res*. **1998**, *37*, 2618−2622.
(23) Rao, R. S.; Walters, A. B.; Vannice, M. A. *J. Phys. Chem. B* **2005**, *109*, 2086−2092.
(24) Ovesen, C. V.; Clausen, B. S.; Hammershoi, B. S.; Steeffensen, G.; Askgaard, T.; Chorkendorff, I.; Norskov, J. K.; Rasmussen, P. B.; Stoltze, P.; Taylor, P. *J. Catal*. **1996**, *158*, 170−180.
(25) Koryabkina, N. A.; Phatak, A. A.; Ruettinger, W. F.; Farrauto, R. J.; Ribeiro, F. H. *J. Catal*. **2003**, *217*, 233−239.
(26) Puzari, A.; Baruah, J. B. *J. Mol. Catal. A* **2002**, *187*, 149−162.

10.1021/cm060241r CCC: $33.50
Published on Web 07/04/2006

developed and presented in the literature.[1,21,27−32]

For many applications in catalysis, copper is coupled with other metals, giving rise to binary oxidic systems which are used as is or dispersed over a support oxide. The most common such binary system is Cu/ZnO, used in the steam reforming of methanol[18,19,33,34] and methanol synthesis reactions.[16,35−37] In particular, a $Cu/ZnO/Al_2O_3$ catalyst is used in the low-pressure methanol synthesis process developed by ICI.[15] More recently, Cu/Ce catalysts have been developed because of their applications to the combustion of CO and methane, water−gas shift reaction, and reduction of SO_2 by CO,[38−42] besides their superior activity compared to the industrial Cu/ZnO catalysts for the steam-reforming and methanol synthesis reactions.[43]

Our efforts to search for new catalyst systems with improved properties for environmental applications have led us to observe the good activity and selectivity of Ga- and Sn-containing catalysts for the reduction of NO_x by hydrocarbon reductants (HC-SCR process),[44−46] in agreement with other authors.[47−55] With these systems, the activity is shifted toward higher temperature values than those observed with Cu-containing catalysts, and selectivity is improved. Thus, binary Cu/Ga and Cu/Sn oxides dispersed onto a suitable support may well be materials of catalytic interest for some environmental reactions. In particular, improvements in the temperature range of activity and selectivity can be expected from such new formulations.

In the present study, we report on the preparation, surface and bulk characterization, and catalytic activity of Cu/Ga and Cu/Sn binary oxides prepared by dispersing nanosized particles over a silica−alumina support with high surface area and acidity.[56] The influence of the Ga or Sn loading on Cu properties has been investigated by preparing two series of samples with different Cu/Ga(Sn) ratios and studying them by various complementary physicochemical techniques with and without the use of probe molecules reacting with the surfaces. The catalytic activities of the two series of samples for decomposition and reduction of NO_x and for oxidation of CH_4 have been compared to investigate the reducing and oxidizing properties of these new catalytic materials.

2. Experimental Section

2.1. Sample Preparation. The silica−alumina (SA) support was synthesized via a sol−gel method from molecular precursors using pure grade reagents from Fluka and Merck-Schuchardt.[56,57] Tetraethyl orthosilane (TEOS), $Si(OC_2H_5)_4$, and aluminum triisopropylate, $Al(OC_3H_7)_3$, were used as sources of Si and Al, respectively. Base-catalyzed hydrolysis of TEOS was used for the synthesis. The calcined SA contained 12.2 wt % Al_2O_3, as determined by ICP analysis.

The binary oxide systems were obtained by successive adsorption of copper, gallium, and tin salt precursors on the SA support. First, the copper phase was deposited on bare SA, and then the gallium or tin phases were deposited on the resulting material after drying. The detailed preparation procedure to obtain 10 g of the final material is the following. First, 230 mL of a $Cu(C_2H_3O_2)_2 \cdot H_2O$ solution of molar concentration depending on the desired loading of copper in the finite material (from 0.027 to 0.046 M) was gently dropped into a slurry of SA in water (100 mL) and maintained at 313 K and at a pH value of 8 by NH_4OH addition. The suspension was maintained at 313 K for 24 h under stirring and then left to rest at room temperature (r.t.) for 18 h. The powder was then filtered and dried at 393 K for 12 h. Three different Cu-containing materials prepared at increasing copper concentrations (3.7×10^{20}, 4.3×10^{20}, and 5.2×10^{20} $atom_{Cu} \cdot g^{-1}$) were then used as starting materials to deposit the gallium or tin salt precursor. One hundred milliliters of a solution of either $Ga(NO_3)_3 \cdot H_2O$ or $SnCl_4 \cdot 5H_2O$ of molar concentration depending on the desired loading of gallium or tin in the finite material (from 0.02 to 0.1 M for $Ga(NO_3)_3 \cdot H_2O$ and $SnCl_4 \cdot 5H_2O$) was slowly dropped into a slurry (100 mL) of the dried copper-containing powder, at controlled pH and temperature (pH = 8 and T = 273 K). The final suspensions were maintained at 273 K for 1 h under stirring. After filtration, the obtained powders were dried at 393 K for 12 h and eventually calcined at 773 K in air for 4 h. The final materials should contain a total amount of metal of 6.4×10^{20} $atom_{Met} \cdot g^{-1}$, with Ga/Cu and Sn/Cu atomic percent ratios of 25, 50, and 75. The samples were then labeled as CuGa(Sn)25/SA, CuGa(Sn)50/SA, and CuGa(Sn)75/ SA.

(27) Boccuzzi, F.; Chiorino, A.; Martra, G.; Gargano, M.; Ravasio, N.; Carrozzini, B. *J. Catal.* **1997**, *165*, 129−139.
(28) Guerreiro, E. D.; Gorriz, O. F.; Larsen, G.; Arrua, L. A. *Appl. Catal., A* **2000**, *204*, 33−48.
(29) Wang, Z.; Liu, Q.; Yu, J.; Wu, T.; Wang, G. *Appl. Catal., A* **2003**, *239*, 87−94.
(30) Drake, I. J.; Fujdala, K. L.; Baxamusa, S.; Bell, A. T.; Tilley, T. D. *J. Phys. Chem. B* **2004**, *108*, 18421−18434.
(31) Larsen, G.; Noriega, S. *Appl. Catal., A* **2004**, *278*, 73−81.
(32) Cushing, B. L.; Kolesnichenko, V. L.; O'Connor, C. J. *Chem. Rev.* **2004**, *104*, 3893−3946.
(33) Agrell, J.; Boutonnet, M.; Melián-Cabrera, I.; Fierro, J. L. G. *Appl. Catal., A* **2003**, *253*, 201−211.
(34) Lee, J. K.; Ko, J. B.; Kim, D. H. *Appl. Catal., A* **2004**, *278*, 25−35.
(35) Chinchen, G. C.; Waugh, K. C.; Whan, D. A. *Appl. Catal., A* **1986**, *25*, 101−107.
(36) Parris, G. E.; Klier, K. *J. Catal.* **1986**, *97*, 374−384.
(37) King, D. S.; Nix, R. M. *J. Catal.* **1996**, *160*, 76−83.
(38) Martinez-Arias, A.; Hungria, A. B.; Fernandez-Garcia, M.; Conesa, J. C.; Munuera, G. *J. Phys. Chem B* **2004**, *108*, 17983−17991.
(39) Martinez-Arias, A.; Hungria, A. B.; Fernandez-Garcia, M.; Conesa, J. C.; Munuera, G. *J. Power Sources* **2005**, *151*, 32−42.
(40) Park, J.-W.; Jeong, J.-H.; Yoon, W.-L.; Jung, H.; Lee, H.-T.; Lee, D.-K.; Park, Y.-K.; Rhee, Y.-W. *Appl. Catal., A* **2004**, *274*, 25−32.
(41) Wang, X.; Rodriguez, J. A.; Hanson, J. C.; Gamarra, D.; Martinez-Arias, A.; Fernandez-Garcia, M. *J. Phys. Chem. B* **2005**, *109*, 19595−19603.
(42) Marban, G.; Fuertes, A. B. *Appl. Catal., B* **2005**, *57*, 43−53.
(43) Liu, Y.; Hayakama, T.; Suzuki, K.; Hamakawa, S. *Catal. Commun.* **2001**, *2*, 195−200.
(44) Guimon, C.; Gervasini, A.; Auroux, A. *J. Phys. Chem. B* **2001**, *105*, 10316−10325.
(45) Auroux, A.; Sprinceana, D.; Gervasini, A. *J. Catal.* **2000**, *195*, 140−150.
(46) Petre, A. L.; Auroux, A.; Gervasini, A.; Caldararu, M.; Ionescu, N. I. *J. Therm. Anal. Cal.* **2001**, *64*, 253−260.
(47) Haneda, M.; Kintaichi, Y.; Mizushima, T.; Kakuta, N.; Hamada, H. *Appl. Catal., B* **2001**, *31*, 81−92.
(48) Haneda, M.; Kintaichi, Y.; Shimada, H.; Hamada, H. *J. Catal.* **2000**, *192*, 137−148.
(49) Haneda, M.; Kintaichi, Y.; Hamada, H. *Appl. Catal., B* **1999**, *20*, 289−300.
(50) Kung, M. C.; Park, P. W.; Kim, D.-W.; Kung, H. H. *J. Catal.* **1999**, *181*, 1−5.
(51) Park, P. W.; Kung, H. H.; Kim, D.-W.; Kung, M. C. *J. Catal.* **1999**, *184*, 440−454.
(52) Haneda, M.; Kintaichi, Y.; Shimada, H.; Hamada, H. *Chem Lett.* **1998**, 181−182.
(53) Shimizu, K.; Satsuma, A.; Hattori, T. *Appl. Catal., B* **1998**, *16*, 319−326.
(54) Li, Y.; Armor, J. N. *J. Catal.* **1994**, *145*, 1−9.
(55) Teraoka, Y.; Harada, T.; Iwasaki, T.; Ikeda, T.; Kagawa, S. *Chem. Lett.* **1993**, 773−776.
(56) Carniti, P.; Gervasini, A.; Bennici, S. *J. Phys. Chem. B* **2005**, *109*, 1528−1536.
(57) Dragoi, B.; Gervasini, A.; Dumitriu, E.; Auroux, A. *Thermochim. Acta* **2004**, *420*, 127−134.

For comparative purposes, three simple oxide samples (Cu/SA, Ga/SA, and Sn/SA) were prepared analogously.

2.2. Characterization Techniques and Procedures. The Al, Si, Cu, Ga, and Sn contents of the samples were measured by ICP (inductively coupled plasma, from Spectro) after dissolving the sample in aqua regia and HF, and then in a solution of HCl.

The surface area values were determined by conventional N_2 adsorption at 77 K using a Micromeritics sorptometer. The samples (0.05 g) were pretreated at 673 K overnight under vacuum (ca. 16 h, 10^{-5} mbar) to remove moisture before analysis.

Transmission electron micrographs (TEM) were obtained with a JEOL JEM-2010 microscope operated at 200 kV.

XRD diffraction analyses of the powder samples were carried out in a Philips PW1710 vertical goniometric diffractometer using Ni-filtered Cu Kα_1 radiation ($\lambda = 1.54178$ Å). The chamber rotated around the sample at 1° (2θ)·min^{-1}; the range of investigation was from 5 to 75° (2θ).

The XPS analyses were carried out with a Kratos spectrometer (model Axis Ultra) using focused monochromatized Al Kα radiation (1486.6 eV) under a residual pressure of 10^{-9} mbar and operating with a constant pass energy of 40 eV for the high-resolution spectra. The analyzed area of the samples was 300 μm × 700 μm. Charge neutralization was used for all measurements, to compensate for charge effects. The binding energy (BE) scale was calibrated using the Si 2p of the silica−alumina support at 103.0 eV (this value was determined for the pure silica−alumina support using the C 1s peak of adventitious carbon at a binding energy of 284.6 eV). The XPS signals were analyzed using a nonlinear Shirley-type background.[58] The samples were pretreated at 673 K under He before the analysis. The fitting peaks of the experimental curves were calculated using a combination of Gaussian (80%) and Lorentzian (20%) functions. The atomic ratios were calculated with the Kratos software with the Scofield intensity factors.

The CO adsorption IR spectra were recorded using a Bruker Vector 22 FTIR spectrophotometer (DTGS detector). The range and resolution of acquisition were 4000−1000 and 2 cm^{-1}, respectively. A self-supporting sample disk (15−20 mg, 18 mm diameter) was first activated in the IR cell at 653 K in oxygen flow for 16 h, then evacuated at the same temperature for 1 h, and finally exposed to CO (Air Liquide >99.9%, 27 mbar) at 298 K. The desorption was carried out for 30 min at r.t. and then at 323, 373, 423, and 473 K. The spectra were recorded at r.t. before and after adsorption and desorption at each temperature.

The heats of adsorption of CO were measured at 303 K in a heat flow microcalorimeter of the Tian-Calvet type, C80 from Setaram, linked to a glass volumetric line to permit the introduction of successive small doses of gas over the powder sample pretreated at 673 K under vacuum (10^{-5} mbar) for 16 h. The equilibrium pressure attained after each CO introduction was measured by a differential pressure gauge (Datametrics). Successive doses were sent onto the sample until a final equilibrium pressure of 0.8 mbar was obtained. The samples were then evacuated for 1 h at the same temperature, and a second adsorption run was performed. The amount of CO irreversibly adsorbed (V_{irr}) was calculated at 0.27 mbar by subtraction of the primary and secondary adsorption isotherms.

Temperature-programmed reduction experiments (TPR) were performed using a TPD/R/O-1100 instrument (CE Instruments). The samples were initially pretreated in air flow (45 mL·min^{-1}) at 623 K for 1 h. After cooling to r.t., the H_2/Ar (4.98% v/ v) reducing mixture flowed through the sample at 15 mL·min^{-1} while the temperature increased from 313 to 1123 K at a constant rate of 8 K·min^{-1}. The H_2 consumption was detected by a thermal conductivity detector (TCD). Peak areas were calibrated with pure H_2 injections (Sapio-Italy, 6.0 purity). Decomposition of the experimental curves was performed by the PeakFit-v4 routine (SeaSolve Software Inc.) searching for the optimum combination of Lorentzian and Gaussian bands.

2.3. Catalytic Activity. The catalysts were tested in a continuous reaction line set up for reactions of reduction and decomposition of nitrogen oxides as already described elsewhere.[2,59] Reductions of NO and N_2O by C_2H_4 and CH_4, respectively, N_2O decomposition, and CH_4 oxidation were studied. Lean conditions were chosen for the feed concentrations of NO, N_2O, C_2H_4, and CH_4, which were set to 1500 ppm. The reactions were carried out under an oxygen-rich atmosphere (O_2 concentration of 15000 ppm), except for N_2O decomposition which was performed under an inert atmosphere. After in situ pretreatment (623 K in 20% O_2/He stream for 4 h) of the samples (0.3 g sieved as 45−60 mesh particles), the reactions were carried out at fixed contact time of 0.360 s in the 673−873 K temperature range. An on-line FTIR spectrophotometer (Bio-Rad with DTGS detector) was used for the qualitative and quantitative analyses of the reactor output streams.

3. Results and Discussion

3.1. Preparation. Identical total amounts of Cu and Ga or Sn metal precursors were used to prepare the Cu/Ga and Cu/Sn binary oxide materials and the reference Cu, Ga, and Sn simple oxides, corresponding to a surface metal density (D_{Met}) of 1.6 atom$_{Met}$·nm^{-2}. This optimum surface metal density has been determined by comparing a set of catalysts with different CuO_x concentrations varying in a wide range, from 0.04 to 3.7 atom$_{Met}$·nm^{-2}; in this series, the sample with 1.6 atom$_{Met}$·nm^{-2} was found to have the best activity for the SCR of NO_x.[3]

All the materials were prepared by depositing the metal precursors on the SA oxide support by an adsorption method. For the binary oxides, successive adsorptions were performed, as schematized in Figure 1. The first step in the preparation of the six binary catalysts was to obtain dry Cu-containing materials (blue sections of Figure 1), after which the salt precursors of gallium or tin (green and orange sections of Figure 1, respectively) were deposited. Because the actual surface metal density of each sample is governed by the affinity of the SA support for the metal precursor, the final materials present D_{Met} values different from 1.6 atom$_{Met}$·nm^{-2} (Table 1). SA showed the highest affinity for the copper phase and the lowest affinity for the gallium phase (D_{Met} for Ga/SA, 0.7 atom$_{Ga}$·nm^{-2}).

All the catalysts have large surface areas (in the 350−500 m^2·g^{-1} interval, Table 1), as expected considering the very high surface area of the SA support (777 m^2·g^{-1}). Moreover, independently of the nature of the deposited oxide, the plot of the surface area of the samples as a function of their total surface metal density followed a decreasing linear trend (Figure 2). This trend could be indicative of the coverage of the support by a phase of much lower surface area which covered pores or interparticle voids.

The TEM images revealed large uncovered portions of the surface and very small metal aggregates, barely detect-

(58) Shirley, D. A. *Phys. Rev. B* **1972**, *5*, 4709−4714.

(59) Bennici, S.; Gervasini, A. *Appl. Catal., B* **2006**, *62*, 336−344.

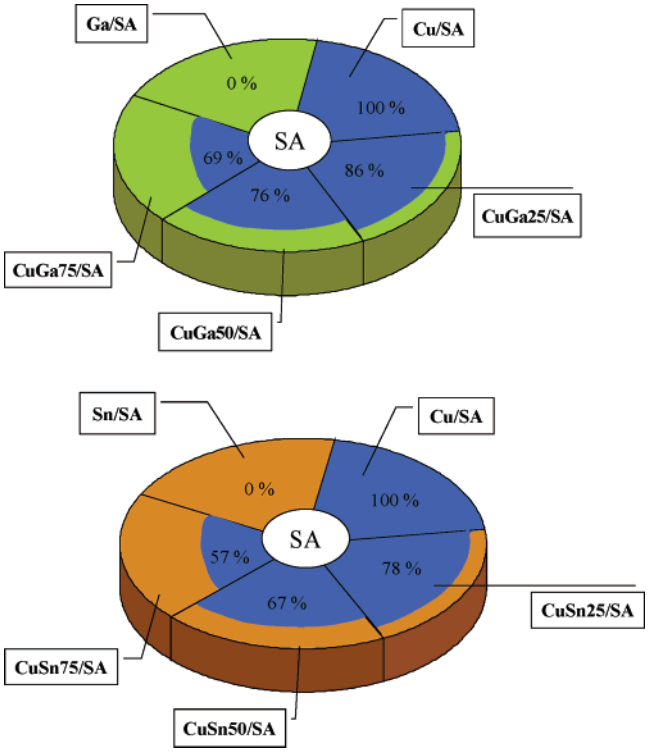

Figure 1. Pie representation of the compositions of the two series of oxide catalysts prepared by dispersing the metal phases on SA support (CuGa/SA and CuSn/SA); each slice corresponds to a sample. Blue color is associated with copper, green with gallium, and orange with tin. Copper atomic percentages are indicated.

Table 1. Metal Content, Metal Density, and Surface Area of the Samples

	metal content				
code	Cu (wt %)	Sn or Ga (wt %)	Sn or Ga (at. %)[a]	D_{Met} ($atom_{Met}$·nm^{-2})[b]	S.A. (m^2·g^{-1})
Cu/SA	6.5		0	1.6	385
CuGa25/SA	4.70	0.84	14	1.3	394
CuGa50/SA	3.96	1.39	24	1.4	351
CuGa75/SA	3.47	1.74	31	1.2	399
Ga/SA		3.88	100	0.7	513
CuSn25/SA	4.19	2.2	22	1.3	405
CuSn50/SA	4.12	3.73	33	1.3	434
CuSn75/SA	3.29	4.69	43	1.2	443
Sn/SA		9.12	100	1.0	456

[a] Cu atomic percent represents the complement to Ga or Sn. [b] Total surface metal density (Cu + Ga(Sn)).

able. Figure 3 shows the TEM images at the same magnification for the Cu/SA, CuGa50/SA, and CuSn50/SA surfaces; the dark zones correspond to CuO in every case. A higher magnification image of the Cu/SA surface is shown in the inset of Figure 3a; at this resolution, particles of CuO of 2−3 nm in size emerge. No gallium or tin oxide aggregates could be individuated in any case, probably due to the very high dispersion of these two oxides.

The XRD spectra of all the oxide samples were dominated by a very broad band in the 20−30° 2θ interval, typical of unstructured silica presence. These spectra are typical of powders with amorphous character, with the absence of separate ordered oxidic phases or metal oxide clusters, as expected on the basis of the high dispersion of the metal oxides observed from TEM results. Lines at positions typical of the SnO_2 phase (26.7°, 34.1°, and 52.2° 2θ) were detected for Sn/SA only.

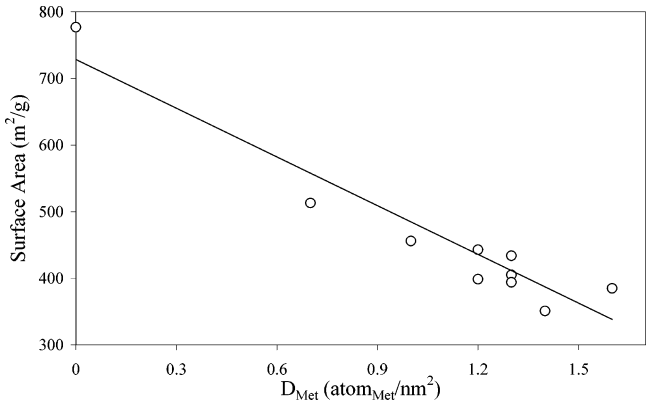

Figure 2. Plot of the BET surface area (S.A.) of the samples as a function of their total surface metal density (D_{Met}, expressed in $atom_{Met}$·nm^{-2}).

3.2. Characterization. (*a*) *XPS*. The SA oxide used as support presented an atomic Si/Al ratio of 4.3, as measured by XPS. This ratio is lower than that expected from the Al_2O_3 content measured by ICP (Si/Al = 6.1)[56] relevant to a homogeneous distribution of Al_2O_3 in the silica. In all cases, the deposition of the metal oxide phases led to a very marked, for Sn/SA, or lighter, for Cu/SA and Ga/SA, increase in the atomic Si/Al surface ratio (Table 2). The Al sites of the support acted as acid sites for the adsorption of Cu, Ga, and especially Sn metal precursors, which selectively deposited on the Al_2O_3-rich zones of the support. The measured Si/Al ratios of the two series of samples (Cu/Ga and Cu/Sn) varied between 6 and 9, without any clear trend with respect to the Cu, Ga, or Sn loading. However, the measured Cu/(Si + Al) surface ratios were around 0.06 for the three samples of the Cu/Sn series while they were lowered to around 0.04−0.03 for the Cu/Ga series (0.07 for Cu/SA). From this behavior, it appears that the Ga phase preferentially covered the Cu phase previously deposited on SA.

A deeper inspection of the electronic situation of the surface metal species has been undertaken by measuring the binding energies in the intervals 950−930 eV for Cu (Figure 4), 1150−1110 eV for Ga, and 500−480 eV for Sn. All the samples containing Cu showed a broad and convoluted XPS band (Cu $2p_{3/2}$) around 934 eV, along with a shake-up satellite associated with Cu(II)[8,60,61] which was more or less well detectable (Figure 4a−4g). This XPS band could be decomposed into two main contributions, one around 933 eV and the other at 935 eV. The presence of the low-energy contribution (typical of Cu(I) and/or Cu(0) species) corresponds mainly to the reduction of Cu(II) by the X-ray beam. Indeed, the intensity of this component is a function of the irradiation time. For the CuGa/SA series, the intensity of the band assigned to reduced copper increases with the Ga content (Table 2 and Figure 4b−4d). This could come from the presence of very small copper aggregates that could be more easily reduced under the X-ray flux. Indeed, Ga seems to induce a decrease of the size of the Cu aggregates.

The high-energy contribution of the XPS band was at a value of BE higher than typical for CuO (934 eV) and can

(60) Espinos, J. P.; Morales, J.; Barranco, A.; Caballero, A.; Holgado, J. P.; Gonzalez-Elipe, A. R. *J. Phys. Chem. B* **2002**, *106*, 6921−6929.
(61) Indovina, V.; Occhiuzzi, M.; Pietrogiacomi, D.; Tuti, S. *J. Phys. Chem. B* **1999**, *103*, 9967−9977.

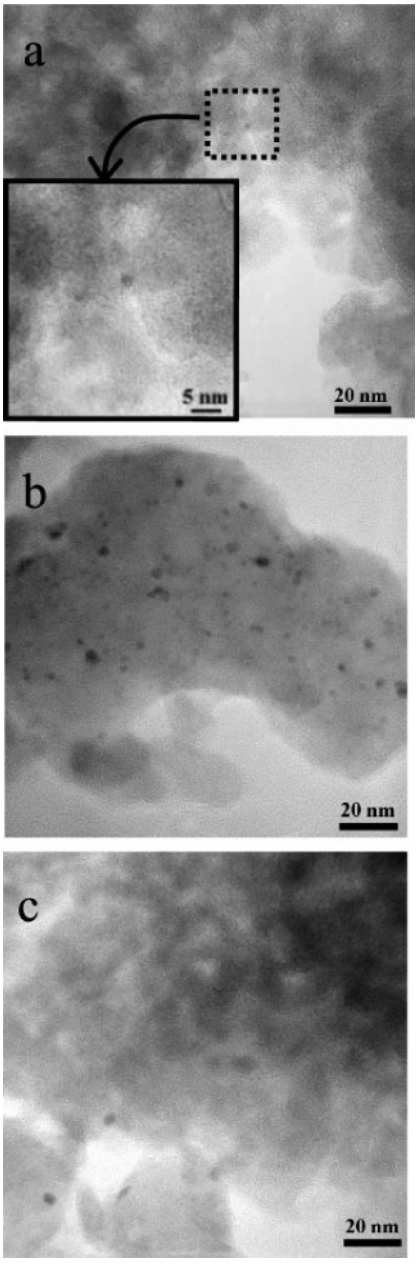

Figure 3. Transmission electron micrograph (TEM) images for Cu/SA (a), CuGa50/SA (b), and CuSn50/SA (c) collected at the same magnification. The inset of section (a) contains an image at higher magnification of a zone of Cu/SA surface.

be associated with well-dispersed Cu(II) metal species interacting with the oxide support (Cu−O−Si−O−).[62] Table 2 reports the binding energy values for Ga $2p_{3/2}$, Sn $3d_{5/2}$, and Cu $2p_{3/2}$ together with the ratios of the satellite to the primary Cu $2p_{3/2}$ peak for Cu(II) (Cu(0) and Cu(I) have no satellite structure).

It appears that the satellite/main peak ratio tends to decrease with the increasing of Ga concentration. This decrease of the satellite/main peak ratio can be related to a decrease in the particle size,[63,64] which agrees with the easier reduction of the smallest Cu particles. Thus, the presence of the Ga phase influenced the electronic behavior and the particle size of the copper species. Specific interaction between Cu and Ga has recently been observed on a series of $Cu/Ga_2O_3-Al_2O_3$ mixed oxide catalysts. The valence band regions of Cu and Ga are not widely separated, and therefore some overlap between the two metals can be expected.[65]

Table 2. XPS Peak Positions for the Studied Samples

		binding energies (eV)[b]				
code	Si/Al[a]	Sn $3d_{5/2}$	Ga $2p_{3/2}$	Cu $2p_{3/2}$		I_{sat}/I_{pp}[d]
SA	4.3					
Cu/SA	7.1			932.9 (20)[c]	935.3 (80)[b]	0.7
CuGa25/SA	6.6		1118.1	933.0 (35)	935.4 (65)	0.6
CuGa50/SA	7.3		1118.1	932.8 (60)	935.3 (40)	0.5
CuGa75/SA	8.0		1118.1	932.7 (70)	934.4 (30)	0.5
Ga/SA	7.8		1118.3			
CuSn25/SA	5.9	486.6		932.9 (30)	935.1 (70)	0.6
CuSn50/SA	8.8	486.9		933.4 (20)	935.5 (80)	0.75
CuSn75/SA	6.7	486.8		932.6 (30)	934.7 (70)	0.5
Sn/SA	15.6	487.2				

[a] Atomic ratio. [b] Al 2p was measured at 74.7 ± 0.1 eV. [c] Relative intensity of the component. The satellite bands of $Cu2p_{3/2}$ (CuII) have been taken into account for the calculation. [d] Intensity ratio of the satellite to the primary peak of the Cu $2p_{3/2}$ for Cu(II).

No variations were observed in the shape and position of the Ga $2p_{3/2}$ (1118 eV, Ga^{3+} species) and Sn $3d_{5/2}$ (487 eV, Sn^{4+} species) XPS bands for the Cu/Ga and Cu/Sn series of samples (Table 2).

(*b*) *FT-IR of Adsorbed CO.* The carbonylic stretchings of CO adsorbed on Cu (I or II) and Ga(III) species give rise to absorptions at different wavenumbers, around 2158−2156 and 2230−2210 cm^{-1},[66−68] respectively, while tin species, even in a reduced state, are not able to stabilize CO.[69] The main IR bands of the carbonylic stretching recorded under 27 mbar of CO for the three samples Cu/SA, CuGa50/SA, and CuSn50/SA are shown in Figure 5a. In every case, the main absorption was centered at 2157 cm^{-1}, with a low-frequency shoulder at 2183 cm^{-1} clearly detectable only for Cu/SA and CuGa50/SA, indicating that CO adsorbed only on copper centers. Since it is well-known that CO cannot be adsorbed on Cu(II) sites at r.t., the 2157 cm^{-1} band can be assigned to CO adsorbed on Cu(I) sites. In particular, molecular monocarbonyl, Cu(I)−CO, and geminal dicarbonyl, $Cu(I)-(CO)_2$, adducts could be responsible for the absorptions at 2157 and 2183 cm^{-1}, respectively.[66,67,70] To study in greater depth the electronic situation of the surface copper species, the three samples were outgassed first at r.t. and then successively at increasing temperatures in the 323−473 K interval, as reported in Figure 5b for Cu/SA. Because the adsorption of CO on Cu(I) is known to be completely irreversible after outgassing at r.t., the reversibly adsorbed

(62) Auroux, A.; Gervasini. A.; Guimon, C. *J. Phys. Chem. B* **1999,** *103*, 7195−7205.
(63) Klein, J. C.; Li, C. P.; Hercules, D. M.; Black, J. F. *Appl. Spectrosc.* **1984**, *38*, 729−734.
(64) Moretti, S.; de Rossi, S; Ferraris, G. *Appl. Surf. Sci.* **1990**, 45, 341−349.
(65) Mathew, T.; Yamada, Y.; Ueda, A.; Shioyama, H.; Kobayashi, T. *Appl. Catal., A* **2005**, *286*, 11−22.
(66) Borgard, G. D.; Molvik, S.; Balaraman, P.; Root, T. W.; Dumesic, J. A. *Langmuir* **1995**, *11*, 2065−2070.
(67) Scarano, D.; Bordiga, S.; Lamberti, C.; Spoto, G.; Ricchiardi, G.; Zecchina, A.; Otero Arean, *C. Surf. Sci.* **1998**, *411*, 272−285.
(68) Rodriguez Delgado, M.; Morterra, C.; Cerrato, G.; Magnacca, G.; Otero Arean, C. *Langmuir* **2002**, *18*, 10255−10260.
(69) Riguetto, B. A.; Bueno, J. M. C.; Petrov, L.; Marques, C. M. P. *Spectrochim. Acta A* **2003**, *59*, 2141−2150.
(70) Spoto, G.; Zecchina, A.; Ricchiardi, G.; Martra, G.; Leofanti, G.; Petrini, G. *Appl. Catal., B* **1994**, *3*, 151−172.

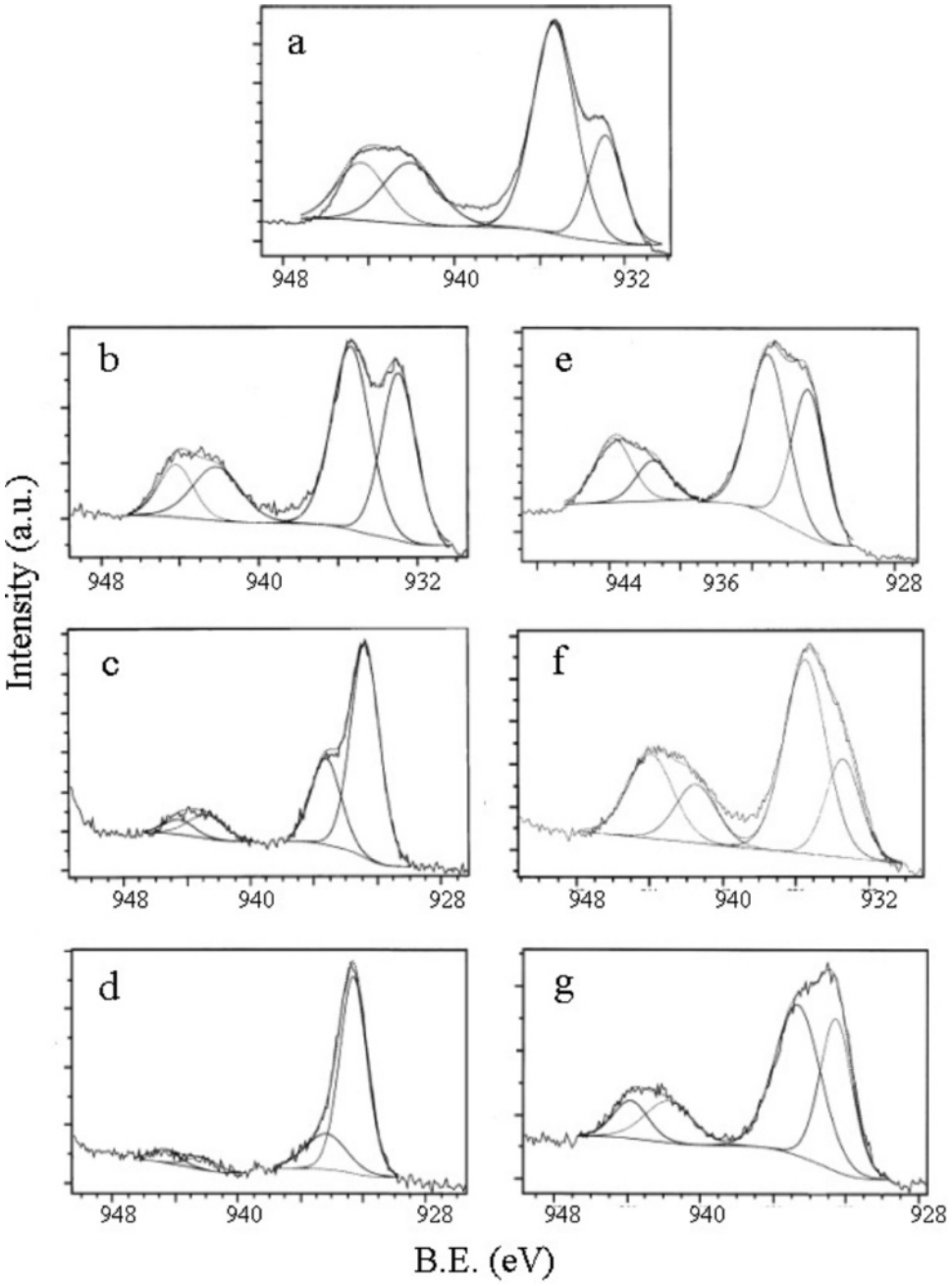

Figure 4. Cu 2p XP spectra of the Cu/SA (a), CuGa25/SA (b), CuGa50/SA (c), CuGa75/SA (d), CuSn25/SA (e), CuSn50/SA (f), and CuSn75/SA (g) oxide samples.

fraction, indicated by the difference between the gray and brown lines in Figure 5a (ca. 50%), could be indicative of the presence of Cu(δ^+) ions (with $1 < \delta < 2$). On these species, CO was stabilized with an interaction energy lower than that on Cu(I) species, due to their lower electron density. The residual band (brown line in Figure 5b), i.e., the fraction which remained on the surface after outgassing at r.t., corresponded to CO absorbed on Cu(I) species. Upon outgassing at higher temperatures, the 2157 cm^{-1} band progressively decreased, and after desorption at 473 K it completely disappeared. The high interaction energy of the Cu(I)−CO adducts, as evidenced by these IR results, is in agreement with the high enthalpy of CO adsorption measured by microcalorimetry.

(*c*) *Adsorption Microcalorimetry.* The uptakes and interaction energies of CO adsorbed on different samples were determined by adsorption calorimetry at 303 K. The three selected samples, Cu/SA, CuGa50/SA, and CuSn50/SA, were studied comparatively. The equilibrium isotherms and differential heats of CO adsorption are shown in Figures 6 and 7, respectively. As shown by the IR spectroscopy results, only the copper phase could adsorb CO, while neither the Ga nor the Sn phases were able to chemically interact with it, in the range of pressure and temperature studied. Therefore, the scale of CO uptake can be put in relation to the amounts of dispersed copper species, Cu(I) and Cu(δ^+), available at the surface. At 0.27 mbar, the amounts of CO adsorbed were 125 $\mu mol_{CO} \cdot g^{-1}$ for Cu/SA, 100 $\mu mol_{CO} \cdot g^{-1}$ for CuSn50/SA, and 69 $\mu mol_{CO} \cdot g^{-1}$ for CuGa50/SA (Figure 6). This order is in agreement both with the total amounts of copper loaded on the SA support and with the copper surface concentrations determined by XPS (Cu/(Si + Al)

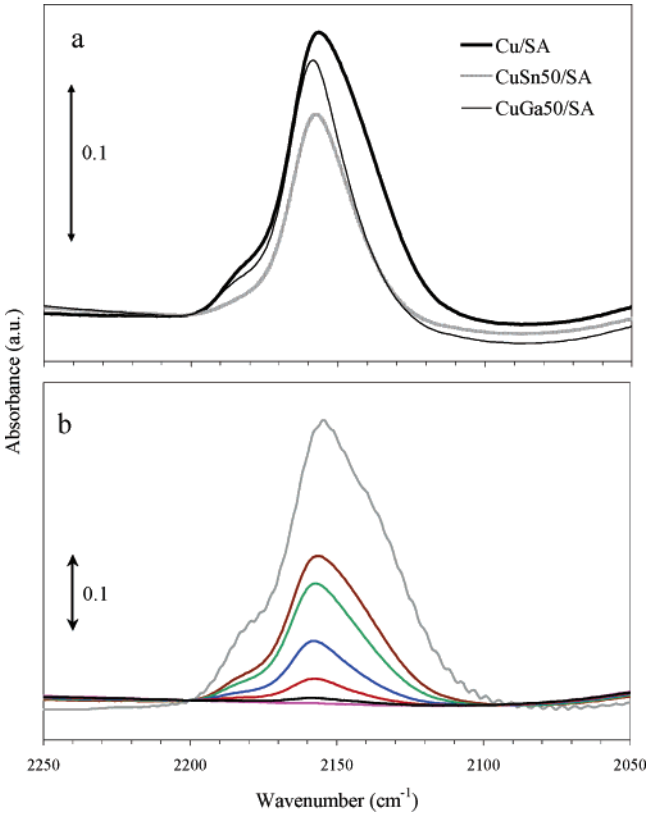

Figure 5. Section **a:** IR spectra of the oxidized Cu/SA, CuGa50/SA, and CuSn50/SA samples collected at room temperature (r.t.) after CO adsorption (27 mbar for 10 min at r.t) and outgassing for 310 min at the same temperature. Section **b**: IR spectra of the oxidized Cu/SA sample collected at r.t. after O_2 pretreatment and outgassing (pink curve), 27 mbar of CO (grey curve), outgassing at r.t. (light brown curve), at 323 K (green curve), at 373 K (blue curve), at 423 K (red curve), and at 473 K (black curve).

surface ratios). As a first approximation, the amounts of CO irreversibly retained by each surface (V_{irr}) could be related to specifically the Cu(I) species. The following order was found for these amounts (Figure 6): Cu/SA (62 $\mu mol_{CO} \cdot g^{-1}$) > CuSn50/SA (53 $\mu mol_{CO} \cdot g^{-1}$) > CuGa50/SA (33 $\mu mol_{CO} \cdot g^{-1}$). The proportion of irreversibly adsorbed CO is always around 50% of the total, and it does not vary appreciably with the nature of the CO-oxide (Ga_2O_3 or SnO_2) coupled with CuO, as the support is the key ingredient governing the distribution of the copper species.

Concerning the interaction energy of CO with the copper species, the measured initial heats were around 105−115 kJ·mol^{-1} for all three samples, and the adsorption heats then regularly decreased down to 15−30 kJ·mol^{-1} with CO coverage, following the order of copper enrichment at the surface (at first CuGa50/SA, followed by CuSn50/SA and then Cu/SA; see Figure 7). The rather high initial adsorption heats confirm the abundant presence of Cu(I) species, strongly interacting with CO.

(*d*) *TPR.* The reduction properties of the oxide phases were evaluated by TPR analysis. The shape and the characteristic parameters of the obtained reduction profiles are indicative of the properties (e.g., particle size) of the different phases deposited on the support. CuO is known to be an easily reducible phase, and the lower the size of the aggregates, the lower the reduction temperatures (T_{max}) observed.[3,71] The reduction of SnO_2 is known to proceed through the formation of metastable SnO, while Ga_2O_3 is known to be resistant to reduction under mild conditions.

Figure 8a shows the TPR profile of the Cu/SA sample, in which the typical shape of the TPR curve accounts for small CuO aggregates dispersed on the SA oxide support:[72] The curve presents a sharp peak at low temperature (500 K, Table 3), attributed to the reduction of free CuO, followed by a long tail up to 660 K, attributed to CuO in interaction with the support (three peaks). The reduction of CuO to Cu(0) was complete, as expected considering the low concentration and small particle size of CuO.[3,72]

Much more complex TPR profiles were obtained for the binary oxide materials (Figure 8b−8g). The obtained profiles correspond to a superposition of TPR profiles of CuO and of Ga_2O_3 or SnO_2. In each TPR curve, the contribution of CuO can be individuated by decomposing the experimental curve on the basis of the reduction profile of Cu/SA (Figure 8, blue lines). The positions of the CuO reduction peaks did not significantly vary upon addition of the second oxide component (Table 3), while the relative proportions among the peaks varied, in particular for the Cu/Ga series of catalysts. Once the reduction peaks of CuO are individuated, the remaining peaks could then be assigned to the reduction

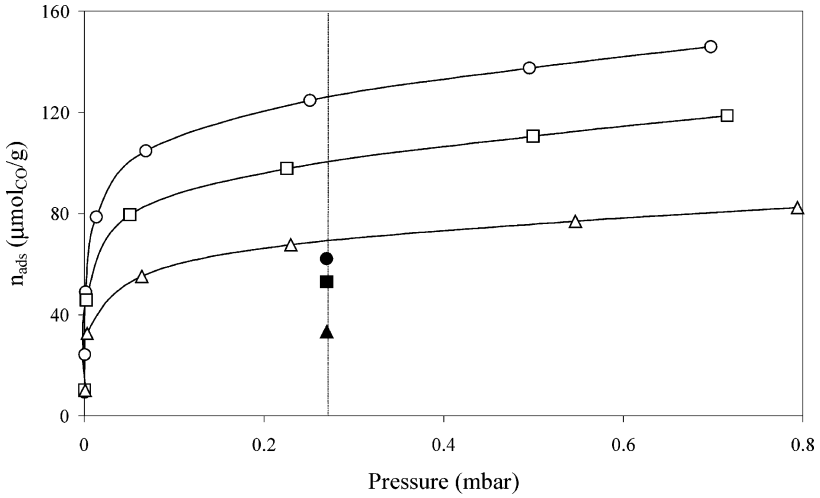

Figure 6. Equilibrium isotherms of CO adsorption on Cu/SA (circle), CuGa50/SA (triangle), and CuSn50/SA (square) oxide samples collected at 303 K (open symbols). Filled symbols represent the amount of CO irreversibly retained by each sample, V_{irr} ($\mu mol_{CO} \cdot g^{-1}$).

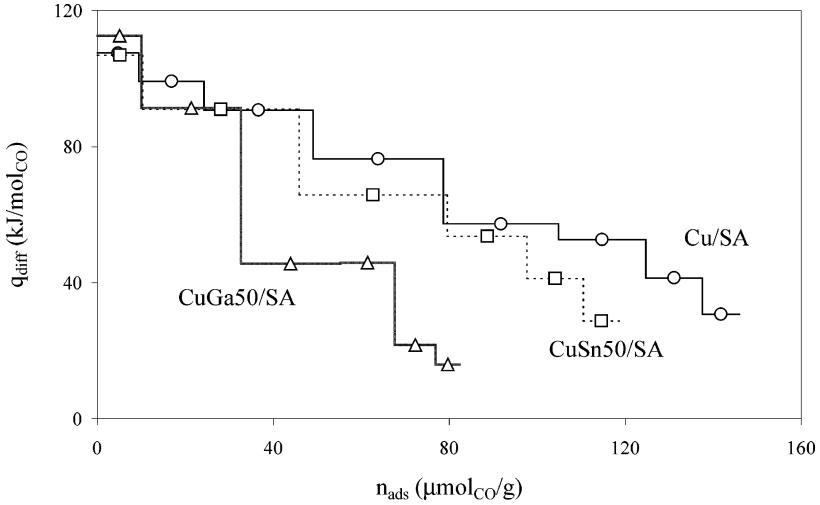

Figure 7. Differential heats (q_{diff}) of CO adsorption versus coverage (n_{ads}) for the Cu/SA (circle), CuGa50/SA (triangle), and CuSn50/SA (square) oxide samples collected at 303 K.

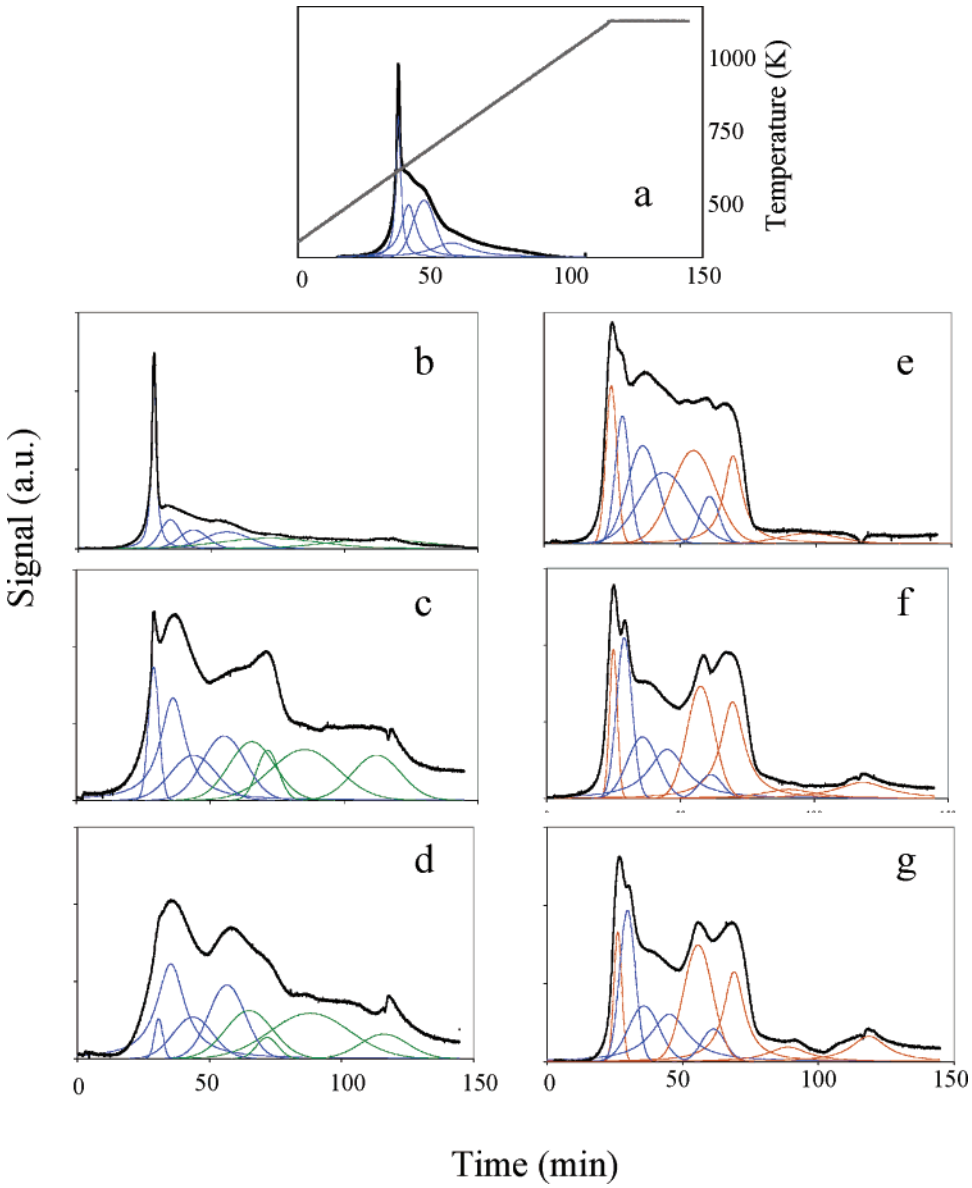

Figure 8. Reduction profiles at increasing programmed temperatures (heating rate 8 K min^{-1}) in the temperature interval 303−1073 K versus analysis time for Cu/SA (a) (the right axis reports the Temperature−Time program used) and for the two series of binary oxides: CuGa25/SA (b), CuGa50/SA (c), CuGa75/SA (d), CuSn25/SA (e), CuSn50/SA (f), and CuSn75/SA (g). Experimental TPR curves (black bold lines) and deconvolved peaks (colored lines: copper, blue curve; gallium, green curve; and tin, orange curve).

Table 3. Results of the TPR Experiments

code	T_{max} (K)[a] Cu	Ga	Sn	reduction ($\mu mol_{H2} \cdot g_{cat}^{-1}$)[b] total	Ga[c]	Sn[d]
Cu/SA	500 530 575 658			879.4 (100)		
CuGa25/SA	468 511 570 657	766 1046		768.7	14.5 (24)	
CuGa50/SA	472 521 574 652	724 764 859 1045		678.4	27.6 (28)	
CuGa75/SA	484 516 574 662	720 767 879 1071		602.2	28.1 (23)	
CuSn25/SA	472 523 577 652		444 692 752 944	800.1		70.4 (38)
CuSn50/SA	473 520 583 669		445 695 751 895 1085	963.0		157.3 (50)
CuSn75/SA	477 519 583 656		453 695 747 884 1089	956.3		219.3 (56)

[a] Temperatures of the TPR peaks calculated by decomposition of the experimental curves. [b] H_2 uptake, the percentage of reduction is indicated in brackets. [c] H_2 uptake calculated for Ga(III) reduction to Ga(I) assuming 100% reduction for CuO. [d] H_2 uptake calculated for Sn(IV) reduction to Sn(0) assuming 100% reduction for CuO.

of Ga_2O_3 (Figure 8, green lines) or SnO_2 (Figure 8, orange lines).

Table 3 summarizes the results obtained in terms of maximum reduction temperatures (T_{max} of the decomposed peaks), total H_2 uptake ($\mu mol_{H2} \cdot g_{cat}^{-1}$), and H_2 uptake for the Ga_2O_3 or SnO_2 reductions, under the assumption that, for every binary oxide sample, the reduction extent of the CuO present was total. The extent of Ga_2O_3 reduction (Ga(III) to Ga(I)) was very low, around 25% for the three Cu/Ga catalysts, without a clear trend with the Ga_2O_3 content. Actually, the TPR profiles of the samples containing Ga indicated that the reduction was still in progress when the highest temperatures were attained.

On the Cu/Sn series samples, the higher the SnO_2 concentration, the higher the calculated extent of SnO_2 reduction (Sn(IV) to Sn(0) reductions of 38, 50, and 56% for CuSn25/SA, CuSn50/SA, and CuSn75/SA, respectively). This accounts for the growth of SnO_2 aggregates, in weaker interaction with the support, and more easily reducible. The reduced samples after the TPR analysis were red, indicating the presence of SnO phase. The complete reduction to metallic tin probably necessitated higher temperatures, as suggested by the incomplete high-temperature peak (1090 K) well-detected in the CuSn50/SA and CuSn75/SA reduction profiles. This high-temperature peak could be associated with the start of a second reduction step (Sn(II) to Sn(0)).

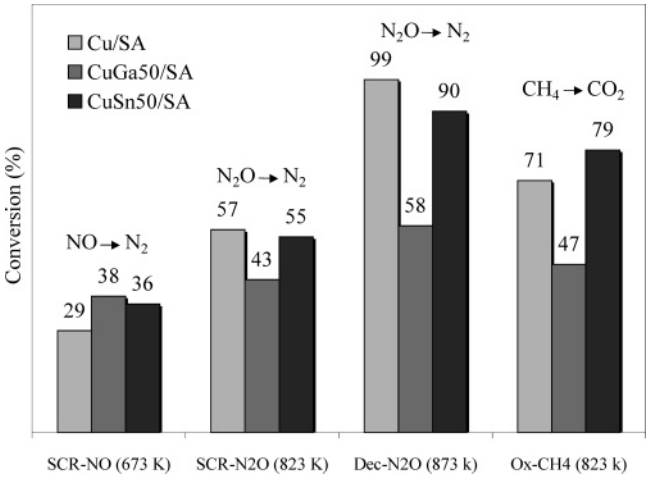

Figure 9. Comparison of the conversions of NO to N_2 in the selective reduction of NO by C_2H_4 (SCR-NO), conversions of N_2O to N_2 in the selective reduction of N_2O by CH_4 (SCR-N_2O), conversions of N_2O to N_2 in the N_2O decomposition (Dec-N_2O), and conversions of CH_4 to CO_2 in the CH_4 total oxidation (Ox-CH_4) reactions over the Cu/SA and binary CuGa50/SA and CuSn50/SA oxide catalysts. The reaction temperatures are indicated in brackets.

3.3. Catalytic Activity. The presence of well-dispersed metal oxide phase of CuO coupled with Ga_2O_3 and SnO_2 can account for some interesting catalytic activity of the prepared materials. We decided to carry out different reactions on the basis of the known catalytic abilities of copper, gallium, and tin oxide surfaces. Reductions of NO and N_2O by hydrocarbon reductants (C_2H_4 and CH_4), direct N_2O decomposition, and CH_4 oxidation were performed as catalytic tests. All the reactions were performed under lean conditions with low reactant concentrations, exploring a wide temperature interval.

For comparative purposes, the obtained results have been summarized in Figure 9 which reports, for each reaction, the percentages of conversion obtained over the Cu/SA, CuGa50/SA, and CuSn50/SA samples at a single temperature. For the selective reduction of NO by C_2H_4 (SCR-NO), the dependence of the conversion of NO to N_2 on temperature followed a typical volcano-shaped curve. The chosen temperature of 673 K was around the point at which the conversion reached its maximum. The selective reduction of N_2O by CH_4 (SCR-N_2O) could proceed at higher temperatures than the SCR-NO because of the more chemically inert characters of N_2O and CH_4 compared with NO and C_2H_4, respectively. In this case, the temperature of 873 K was chosen to make the comparisons. Since the reaction of N_2O decomposition (Dec-N_2O) is known to proceed at very high temperatures, we chose 873 K to make comparisons among the catalytic activities of the catalysts. Finally, the temperature of 823 K was chosen for making comparisons in the reaction of total oxidation of CH_4 (Ox-CH_4).

The addition of the second metal oxide phase (gallium or tin) to copper gave rise to remarkable differences in the catalytic activity. Both binary oxide catalysts (CuGa50/SA and CuSn50/SA) showed higher activities in the SCR-NO reaction than Cu/SA, with NO conversions about 10% higher than those obtained over Cu/SA. In the reduction and decomposition of N_2O (SCR-N_2O and Dec-N_2O, respectively), Cu/SA was the most active catalyst. CuGa50/SA

showed the lowest activities in the reactions where N_2O was concerned because of the low surface concentration of copper, as revealed by the spectroscopic investigations. The presence of tin oxide was favorable for enhancing the oxidative properties of the surface of copper oxide. A higher conversion of methane (by about 10%) was observed over CuSn50/SA than Cu/SA.

From the catalytic investigations performed, it emerges that the addition of a second metal oxide to CuO can impart new properties to the copper surface. The reducing properties can be improved by Ga_2O_3 addition, while SnO_2 improves the oxidative properties. Besides the nature of the added oxide, its loading and interaction with the primary deposited oxide (CuO) play an important role in the development of new active and selective systems, as has been observed.[73]

Conclusions

In this work we confirmed that the surface and catalytic properties of dispersed copper oxide could be influenced by the addition of a second metal oxide. The two series of Cu/Ga and Cu/Sn oxide catalysts prepared, with different Cu/Ga(Sn) proportions, had the metal oxide phases sparsely covering the acidic silica−alumina support. The strong interaction between the primary deposited copper phase and the oxide support led to the formation of well-dispersed partially reduced Cu centers, evidenced by XPS and CO adsorption. The main surface properties of the dispersed metal oxides point to some differences among the two series of samples. The affinity of Ga for the primary deposited copper phase was high and gave rise to active metal−support interactions. In contrast, Sn was deposited preferentially on the bare support, without any interaction with the copper phase.

These differences in the surface properties between the two series of catalysts imparted to the CuO phase enhanced reducing (Cu/Ga) or oxidizing (Cu/Sn) catalytic properties, as evidenced in NO_x reduction and CH_4 oxidation reactions, respectively. It is therefore possible to widen the spectrum of activity of copper oxide surfaces by the suitable addition of a second oxide component that can selectively direct the catalytic activity of the resulting surface.

Acknowledgment. The ICP (P.Mascunan, N.Cristin) and TEM (Mimoun Aouine) analysis services of the Institut de Recherches sur la Catalyse, CNRS, Villeurbanne, France, are gratefully acknowledged.

CM060241R

(71) Torre-Abreu, C.; Ribeiro, M. F.; Henriques, C.; Delahay, C. *Appl. Catal., B* **1997**, *12*, 249−262.

(72) Bennici, S.; Carniti, P.; Gervasini, A. *Catal. Lett.* **2004**, *98*, 187−194.

(73) Bennici, S.; Gervasini, A., in preparation.